Time-domain terahertz study of defect formation in one-dimensional photonic crystals

Hynek Němec, Petr Kužel, Frédéric Garet, and Lionel Duvillaret

One-dimensional photonic crystals composed of silicon and air layers with and without twinning defect (i.e., a periodicity break where one half of the photonic structure is a mirror image of the other one) are studied by means of terahertz time-domain transmission and reflection spectroscopy. The structure with defect is decomposed into building blocks: two twins and a defect. A phase-sensitive characterization in transmission and reflection allows us to fully determine the transfer matrices of any block and consequently to predict the properties of composed structures regardless of the microstructure of the constituting blocks. It is shown and experimentally demonstrated that the defect level position is controlled by the reflectance phase of the twins. Possible approach of the reflectance phase determination by use of Kramers–Kronig analysis is also discussed.

OCIS codes: 300.6240, 230.4170.

1. Introduction

Photonic crystals (PCs) have attracted considerable attention in recent years.[1–3] The PCs are periodic dielectric structures that may exhibit ranges of forbidden frequencies for the propagation of light, so-called photonic band gaps. Such structures were proposed to solve several problems in fundamental research, related, e.g., to the control of spontaneous emission from atoms and molecules and localizing and channeling light.[1,4] The operating range of currently available PCs covers a wide range of frequencies, from the microwaves[5] through the terahertz range[6] up to the visible,[7,8] and they can potentially find many applications in optoelectronics and optical communications.[9,10] One of the topics of major interest for filtering applications and signal demultiplexing is the control of defect modes.[8,11,12]

Up to the present, little attention has been devoted to the full experimental characterization of PCs: In most cases, only the existence of the forbidden gap is verified from the intensity of transmittance or reflectance, and only a few papers report measurements of the related phases. Most of them concern an experimental determination of the transmittance phase in the microwave,[13,14] terahertz,[15,16] and optical[17,18] spectral domains. Indeed, the transmittance phase provides a direct insight into the dispersion relations of the experimentally excited eigenmodes of the photonic structures.[13] On the other hand, a reliable and accurate measurement of the phase of the reflected field, which controls other important properties of photonic structures, like the frequencies of defect modes in PCs with broken periodicity,[19–21] is much more difficult to carry out.[19]

Time-domain terahertz spectroscopy (TDTS) is based on an emission of a picosecond terahertz (THz) pulse and on its synchronous phase-sensitive detection, i.e., it can provide the temporal profile of the electric field of the pulse transmitted or reflected by the investigated sample.[22] The transmission variant of this method is well established; on the other hand, owing to difficulties with accurate determination of the reflectivity phase,[23] the complete characterization of PCs (i.e., a simultaneous determination of transmittance and reflectance phase) has not yet been carried out.

In this paper we take advantage of a recently demonstrated technique allowing a reliable determination of the reflectance phase,[24] and we fully characterize two one-dimensional (1-D) PCs. This allows us to predict frequencies of the defect modes of photonic structures composed of these PCs separated

H. Němec and P. Kužel (kuzelp@fzu.cz) are with the Institute of Physics, Academy of Sciences of the Czech Republic and the Center for Complex Molecular Systems and Biomolecules, Na Slovance 2, 182 21 Prague 8, Czech Republic. F. Garet, L. Duvillaret, and H. Nemec are with the Laboratoire d'Hyperfréquences et de Caractérisation, Université de Savoie, 73376 Le Bourget du Lac Cedex, France.

Received 5 September 2003; revised manuscript received 10 November 2003; accepted 10 December 2003.

0003-6935/04/091965-06$15.00/0

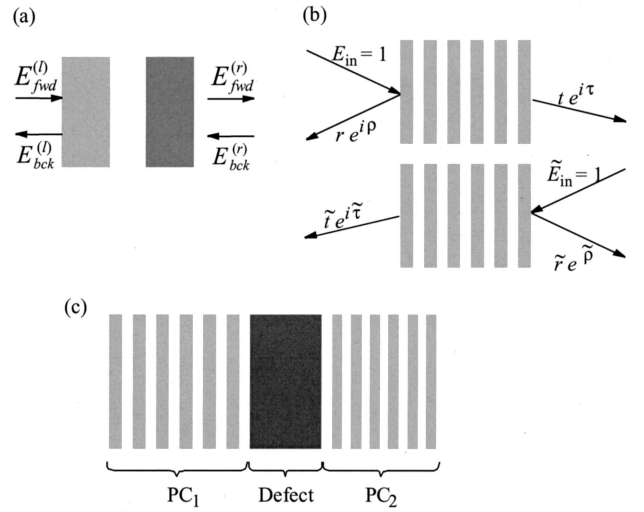

Fig. 1. Schematic definition of (a) fields used in the transfer matrix method, (b) transmission and reflection coefficients for left- and right-hand measurements, and (c) investigated structure.

by a homogeneous layer with varying thickness (twinning defect). Our treatment is general and allows the prediction of bound states in any structures (even aperiodic) exhibiting a forbidden band. 1-D systems were chosen owing to their simplicity; exact analytic expressions for frequencies of defect modes can be easily derived as well as simply understood.[21,25] On the other hand, the ability to completely characterize two- or three-dimensional photonic structures can also be of great interest and could serve as an important tool in the characterization and the design of large-scale devices.[26]

2. Theoretical Description

Our description is based on a transfer matrix formalism[27] that is very often used for the investigation of 1-D PCs. The transfer matrices usually relate the amplitudes of electric fields corresponding to forward- and backward-propagating waves at the interfaces between adjacent layers; we will use the same conventions and definitions as those introduced in Ref. 21. The product of individual transfer matrices yields the transfer matrix of an entire block that connects the fields at the left-hand side of the block [$E^{(l)}$] to those at its right-hand side [$E^{(r)}$] [see Fig. 1(a)]:

$$\begin{bmatrix} E_{\mathrm{fwd}}{}^{(l)} \\ E_{\mathrm{bck}}{}^{(l)} \end{bmatrix} = \underbrace{M_1 M_2 \ldots M_n}_{M} \begin{bmatrix} E_{\mathrm{fwd}}{}^{(r)} \\ E_{\mathrm{bck}}{}^{(r)} \end{bmatrix}. \tag{1}$$

Assuming the block is composed only of nonabsorbing media, the elements of its transfer matrix can be simply identified with the complex reflection and transmission coefficient of the block:

$$M = \frac{1}{t} \begin{Bmatrix} \exp(-i\tau) & r\,\exp[-i(\rho - \tau)] \\ r\,\exp[i(\rho - \tau)] & \exp(i\tau) \end{Bmatrix}, \tag{2}$$

where r and t are the reflectance and transmittance amplitudes and ρ and τ are the corresponding phases, respectively. We have implicitly assumed here that the incident wave impinges on the structure from the left-hand side, i.e., $E_{\mathrm{fwd}}{}^{(l)} \equiv E_{\mathrm{in}}$ and $E_{\mathrm{bck}}{}^{(r)} = 0$ [see top of Fig. 1(b)]. The structure can be alternatively characterized by the complex transmission $\tilde{t}\,\exp(i\tilde{\tau})$ and reflection $\tilde{r}\,\exp(i\tilde{\rho})$ coefficients measured when the incident wave impinges on the structure from the right-hand side: $E_{\mathrm{bck}}{}^{(r)} \equiv \tilde{E}_{\mathrm{in}}$, and $E_{\mathrm{fwd}}{}^{(l)} = 0$ [see bottom of Fig. 1(b)]. One can easily show that $\tilde{t} = t$, $\tilde{\tau} = \tau$, $\tilde{r} = r$, and $\tilde{\rho} = 2\tau - \rho + \pi$. The structure is thus completely characterized by a set of three spectral functions: t, τ, and ρ.

To investigate complex structures (composed, e.g., of several kinds of PCs), it appears that decomposing the structure into several suitable building blocks is useful. Each block then can be described in terms of its transfer matrix [Eq. (2)]. In principle, given the incidence angle and the polarization of the incident wave, the transfer matrix of any block can be calculated if its microstructure (i.e., thickness, refractive index, and wave impedance of each of its constituting layers) is known. However, in practice the microstructure data are not always available and/or the real microstructure can significantly differ from the expected one. In this case phase-sensitive measurements of the complex reflection and transmission coefficients can provide all of the required information. The TDTS is capable of providing all of the entries of Eq. (2) for reasonable real blocks operating in the THz range. Hence the properties of the entire complex structure can be predicted before it is built from the blocks without exact knowledge of the microstructure details. In contrast with most theoretical descriptions, we express the transfer matrices in terms of experimentally accessible quantities, i.e., the reflectance and the transmittance of the separate blocks surrounded by vacuum. One can easily show that the transfer matrix of two such blocks—**A** and **B**—put into optical contact reads simply $\mathbf{A} \cdot \mathbf{B}$.

We apply this approach to a one-dimensional PC, including a twinning defect [Fig. 1(c)]. We consider a structure composed of three blocks: The outer blocks are two periodic PCs—twins (denoted by indices 1 and 2)—and the inner block represents an enclosed defect (index D). In the ideal case, the two PCs have identical properties, as they are assumed to have the same microstructure. However, experimental realizations of these PCs can show different properties, to some extent. The corresponding transfer matrices then could display slightly different coefficients. Depending on the optical thickness of the defect, the whole structure may exhibit a defect mode, i.e., a narrow range of frequencies in the forbidden gap, for which the propagation through the structure is allowed.[28] One finds the following condition for the defect level in the limit of perfect PCs ($r_1 \to 1$ and $r_2 \to 1$):

$$\tilde{\rho}_1 + \rho_2 = 2\pi m - 2\tau_D + 2\,\arg[1 - r_D\,\exp(i\rho_0)], \tag{3}$$

where m is an arbitrary integer and where

$$\rho_0 = \rho_D + \tilde{\rho}_1 = \rho_2 + \tilde{\rho}_D. \tag{4}$$

This last equality is automatically fulfilled at the defect level frequencies. Equation (3) in fact represents the resonance condition in a Fabry–Pérot interferometer: Constructive interference—or equivalently, the defect level—occurs if the phase shift $\tilde{\rho}_1$ due to the reflection on the left "mirror" (PC_1) plus the phase shift ρ_2 due to reflection on the right "mirror" (PC_2) plus twice the phase shift introduced by the propagation through the "resonator" (defect) equals any integer multiple of 2π. The last term of Eq. (3) arises from the fact that the resonator is formally enclosed between infinitesimally thin vacuum layers, e.g., $\tilde{\rho}_1$ describes the reflectance phase for the incident wave coming from the vacuum and not from the defect medium. This term thus accounts for the impedance mismatch between the building blocks and the vacuum.

Equation (3) is not restricted to ideal periodic PCs but can be applied to other structures showing bandgaps, e.g., chirped structures, disordered systems[29] or photonic quasicrystals.[30]

In case the defect consists only in a vacuum layer, Eq. (3) is largely simplified and becomes equivalent to that reported in Refs. 19 and 20: The last term disappears, and the phase shift τ_D is simply expressed as $2\pi f d_D/c$, where f is the frequency, c is the speed of light in vacuum, and d_D is the defect thickness.

Equation (3) clearly shows that the defect position is controlled by the reflectance phases in the forbidden gap of the PCs. It is then crucial to have an experimental access to this parameter to predict the properties of complex structures.

3. Experimental Details

The PCs (outer blocks) were fabricated with use of three 100-μm-thick wafers of high-resistivity silicon ($\rho > 1000\ \Omega$ cm) with a 5-cm diameter (the refractive index of silicon is practically constant in the THz range and equals 3.41). The individual wafers were separated by air layers, which we built by inserting small 350-μm-thick silicon spacers placed near the edges of the wafers. The structure was mechanically stabilized by drops of glue put on its edges. Structures with defect were composed of two such PCs separated by an air layer using spacers with thicknesses ranging from 50 μm up to 1 mm: The entire structure was mechanically clamped during the measurements.

The THz experiments were made by use of setups described in detail in Refs. 24, 31, and 32. (i) The two individual PCs were first completely characterized; the complex transmittance and the reflectance of both structures were measured. The reflection spectra were obtained with use of a novel scheme that allows highly accurate determination of the phase of the reflected wave.[24] (ii) Long temporal scans (250 ps) were acquired for the study of the transmission functions of structures with defect in order to achieve better frequency resolution of the defect levels. Indeed, TDTS is a time-domain method, and its frequency resolution Δf depends essentially on the length T of the temporal window of the scans: $\Delta f T \geq 1$. A resolution better than a few GHz (0.1 cm^{-1}) can hardly be achieved. This is also the reason why we have utilized individual PCs with only three silicon layers; the transmittance in the forbidden gap appreciably decreases with an increasing number of layers. At the same time, the defect spectral lines exhibit a significant narrowing and, consequently, they could not be easily resolved by use of TDTS for a higher number of periods of PCs.

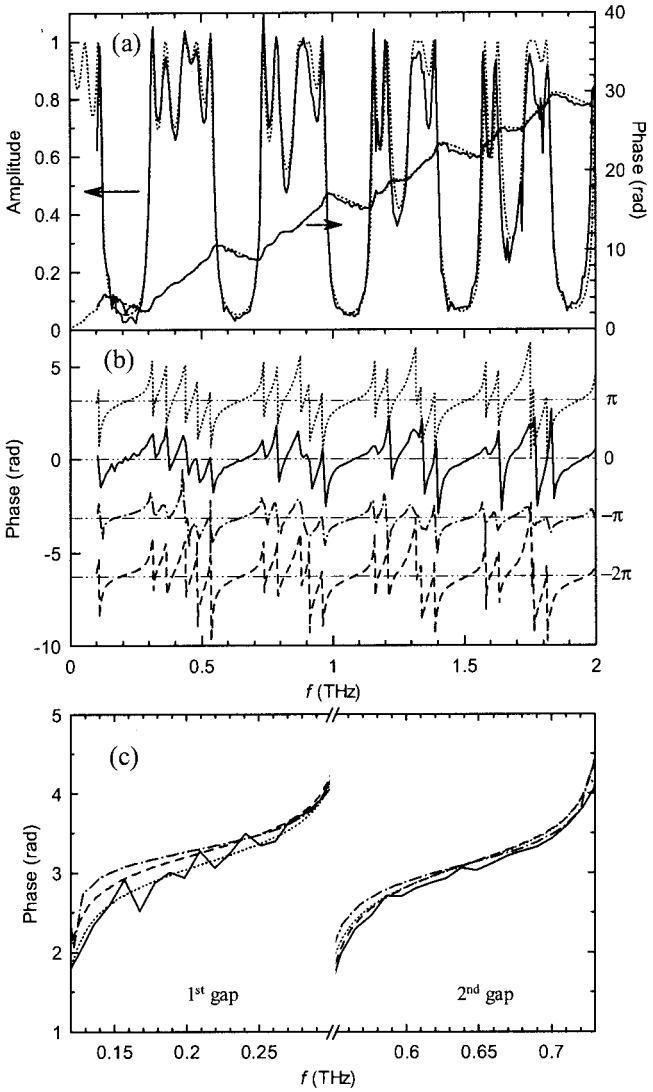

Fig. 2. (a) transmission (amplitude and phase) and (b), (c) reflection (phase) spectra of one of the PCs. The solid curves represent the measured data, whereas the dotted curves correspond to theoretical calculations based on the microstructure. Dashed and dash-dotted curves in (b) and (c) are calculated by means of Kramers–Kronig relations from the theoretical transmittance (dashed curve) and from the measured transmission amplitude (dash-dotted curve). Artificial phase shifts of π in (b) are introduced for graphical clarity only.

4. Discussion

We first characterized the individual PCs composed of three layers of silicon; both reflection and transmission spectra are presented in Fig. 2. The five

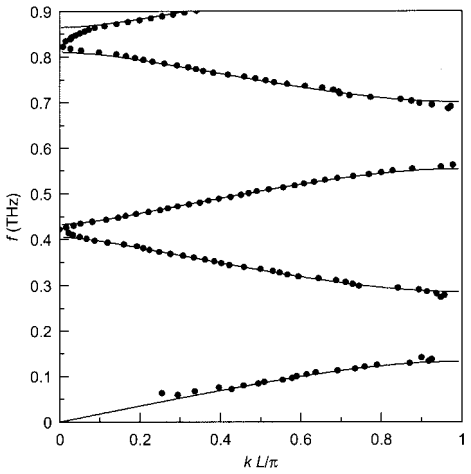

Fig. 3. Dispersion relations for the studied PCs. The symbols are the experimentally determined values for a stack PC_1 + PC_2 separated by a 350-μm spacer (i.e., six-layer PC); the lines are the theoretical predictions for an ideal PC. L is the lattice parameter of the PC (475 μm).

lowest forbidden bands are clearly observed. The microstructure of the PCs was assumed to be known from the fabrication protocol. However, in order to achieve a good agreement between the theoretical curves (i.e., calculated from the microstructure) and the experimental data, it was necessary to increase slightly the thickness of the air layers separating the silicon wafers; the values of 370 μm for PC_1 and 380 μm for PC_2 lead to excellent fits of the measured data [see Fig. 2(a)]. This small increase of air layers is probably due to glue infiltration between the spacers and the silicon wafers. The subsequent calculations are then performed with the following microstructure data:

PC_1: Si(100 μm)/air(370 μm)/Si(100 μm)/air(370 μm)/Si(100 μm),

PC_2: Si(100 μm)/air(380 μm)/Si(100 μm)/air(380 μm)/Si(100 μm).

The transmittance phase of a PC defines its effective refractive index, and thus it directly provides the dispersion relation of the structure.[13] Figure 3 shows the measured dispersion relation of a six-layer PC obtained through a stacking of PC_1 and PC_2 with use of a 350-μm spacer. In this plot the existence of subsidiary forbidden gaps near 415 and 840 GHz (gaps above 1 THz are not shown in Fig. 3) appear. The corresponding transmission minima can be also clearly identified in Fig. 2(a). These additional gaps originate from the small mismatch between the optical thicknesses of Si (341 μm) and air (~375 μm) layers and consequently become well pronounced only for crystals with a large number of periods.

We have already emphasized the key role of the reflectance phase of PCs for the position of the defect levels. In many cases it is rather difficult to measure this parameter directly. The application of the Kramers–Kronig (KK) relations to the measured transmittance and reflectance intensities or amplitudes is therefore the only way to obtain it. As TDTS is able to provide both amplitude and phase spectra, the present research constitutes an excellent opportunity to study the applicability of KK relations for the determination of the reflection phase from the measured amplitudes. The KK relations for the reflectance read[33]

$$\rho(f) = \rho(0) - \frac{2f}{\pi} \mathrm{P} \int_0^\infty \frac{\ln r(f')}{f'^2 - f^2} \, \mathrm{d}f', \tag{5}$$

where P stands for the principal value. If the amplitude transmittance t is measured rather than the reflectance r, one can substitute into Eq. (5):

$$r = \sqrt{1 - t^2}. \tag{6}$$

The reflectance phase behavior is governed mainly by the reflectance amplitude in the frequency ranges where the argument of the integral in Eq. (5) reaches the largest values. Apparently, this can happen in two cases: (i) the denominator vanishes for frequencies approaching f and (ii) the numerator diverges for frequencies where the reflectance vanishes. We are interested mainly in the reflectance phase at frequencies lying in the forbidden gap. The logarithm of reflectivity in the gap is very small for PCs with a reasonably good quality; consequently, the contribution of type (i) is not the leading one. The contribution of type (ii), arising from high-transmission spikes in the regions close to the forbidden gap, is clearly dominating.

For frequencies near the center of the bandgap of a photonic structure, the denominator of the integral argument in Eq. (5) is always far from resonance; the integral itself thus does not show a significant variation for these frequencies. Consequently, the reflectance phase always exhibits a quasi-linear frequency dependence close to the bandgap center. Moreover, a straightforward calculation of $\mathrm{d}\rho/\mathrm{d}f$ leads directly to the conclusion that $\rho(f)$ is an increasing function [except for the singular points $r(f) = 0$, where phase jumps may occur]. Both of these properties are illustrated by our experimental results plotted in Figs. 2(b) and 2(c).

Figures 2(b) and 2(c) show a comparison of the reflectance phases of PC_1 directly measured and calculated with use of different methods and input data. Figure 2(b) indicates a very good overall agreement of all curves in the entire spectral range studied. Figure 2(c) shows details of the behavior in the two lowest photonic gaps. The deviations of the curves from the theoretical one (dotted curve), which is based on the direct calculation from the microstructure data, characterize the precision of the given approach. The experimental curve (solid line) is in quite good agreement with the theoretical one in both gaps. The dashed curve represents the data calculated with use of KK relations from the theoretical amplitude transmittance, i.e., the input data are virtually error free. However, the KK integral is calculated only over a limited frequency range (0.1–2.0 THz). The last curve (dash-dotted curve) is obtained from the

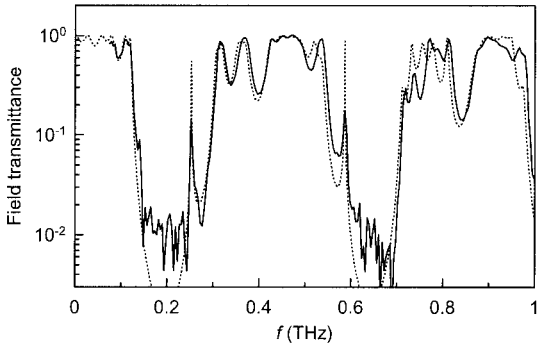

Fig. 4. Transmission spectrum of a photonic structure with defect. Dotted curve, theoretical calculations; solid curve, experiment.

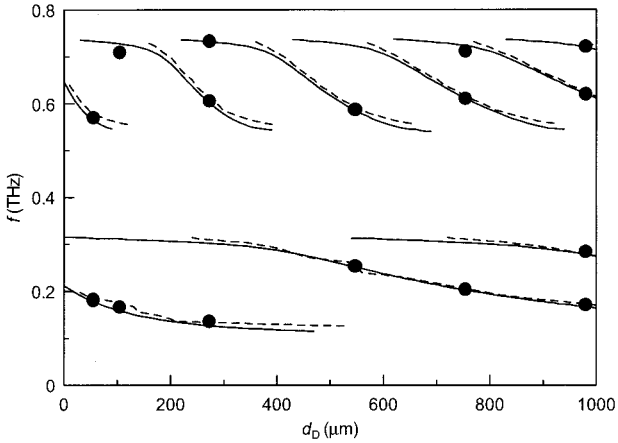

Fig. 5. Frequency of defect modes versus defect layer thickness. Filled circles, measured data; solid curve, prediction based on the microstructure; dashed curve, prediction based on Eq. (3) and on the measured reflectance phases $\tilde{\rho}_1$ and ρ_2.

measured transmittance amplitude with use of KK analysis. A significant discrepancy between this curve and the theoretical one is observed mainly in the lowest gap. This is connected to the fact that the regions that contribute to the KK integral are formed of a series of quite sharp spikes; a high-resolution and highly precise measurement of the transmittance is thus required to supply the input data. The lack of experimental data below 0.1 THz and its reduced precision close to this limit is at the origin of the discrepancy in the lowest gap. On the other hand, the second forbidden gap matches the frequency range giving the highest dynamics of measure of our THz spectrometer, and consequently the agreement is far better.

Let us now analyze the results obtained for the structures with defect. An example of a transmission spectrum of the structure with a 548-μm-thick air-layer defect is shown in Fig. 4. One can clearly identify the defect mode occurring at 252 GHz in the first gap and another one at 586 GHz in the second gap. The experimental peak transmittance at the defect level frequency is almost 1 order of magnitude lower than the one predicted by theory (equals to 1). This is mainly due to the low-frequency resolution of the TDTS (Δf = 4 GHz for 250-ps scans). The calculated FWHM of the defect level is ~1 GHz.

Figure 5 summarizes the dependence of the defect mode frequency on the defect thickness for the two lowest forbidden bands. The points correspond to the frequencies of defect modes identified in the measured transmission spectra. Solid curves show the predictions obtained from numerical calculations based on the system microstructure. For PCs consisting of only three periods, we have verified that the difference between the exact numerical solutions of the problem and the solutions of Eq. (3), for which we assume that $r \rightarrow 1$, is negligibly small. Here again, the thickness of the defect layer has been slightly increased in the calculations (adjustment smaller than 50 μm) compared with the nominal thickness of the spacers in order to fit the experimental data. This can be simply understood in terms of the stress produced while the twins are clamped together. It is important to note that the thickness adjustment has been made just once for each defect thickness, leading to a very good fit of all the measured defect frequencies (e.g., three different frequencies for a 270-μm-thick defect) with the prediction. Finally, the dashed curve indicates the prediction based on Eq. (3) and on the experimentally obtained reflectance phases $\tilde{\rho}_1$ and ρ_2. It is necessary to emphasize that the setup for reflection measurements does not allow us to measure under strictly normal incidence.[24] However, measurements in our experimental conditions (with an incidence angle of 15° and in TM polarization) lead only to a minor systematic shift of the predicted frequencies as compared with the normal incidence.[21] This shift corresponds to the difference between the solid and the dashed curves in Fig. 5. Larger differences are observed if the defect level lies near the bandgap edges; the forbidden gap in fact is shifted to slightly higher frequencies with increasing incidence angle for TM polarization.[21]

The presence or absence of defect modes in the vicinity of the bandgap edges needs to be considered cautiously. As the transmission of real PCs does not decrease steeply, the position of edges is not well defined. In addition, the uncertainty of the position of band edges may be increased by possible small changes of the microstructure of PCs owing to clamping. Hence the beginning and the ending of the lines predicting the frequency of defect modes (Fig. 5) is not well defined, and the experimentally identified defect modes can be confused with the maxima outside the forbidden gap.

The method discussed in this paper can in principle be extended to structures containing dissipating media. The transfer matrices then should be supplied with loss terms, i.e., each transfer matrix would be determined by six independent parameters instead of three. A complete characterization of such a block would be required in turn to measure the spectra from both sides of the block.

5. Conclusion

Two PCs and a PC with twinning defect were completely characterized by TDTS. It was shown and experimentally demonstrated that the defect level position is controlled by the reflectance phase in the bandgap of the twins. The reflection setup of the TDTS was proven to be able to predict properties of structures with defect, regardless of whether the microstructure of constituting blocks (i.e., thicknesses, refractive indices, and wave impedances of the individual layers) is known.

Finally, the measured reflectance phase was compared to that obtained by means of KK relations from the transmittance amplitude; KK analysis yields the correct phase in the bandgap if the amplitude spectra are accurately determined in both neighboring allowed bands.

This work was supported by the French Ministry of Education through an "Action Concertée Incitative," by the Ministry of Education of the Czech Republic (Project No. LN00A032) and by the Volkswagen Stiftung (Grant No. I/75908).

References

1. E. Yablonovitch, "Inhibited spontaneous emission in solid-state physics and electronics," Phys. Rev. Lett. **58,** 2059–2062 (1987).
2. Y. Fink, J. N. Winn, S. Fan, C. Chen, J. Michel, J. D. Joannopoulos, and E. L. Thomas, "A dielectric omnidirectional reflector," Science **282,** 1679–1682 (1998).
3. K. Sakoda, *Optical Properties of Photonic Crystals* (Springer–Verlag, Berlin, 2001).
4. S. John and J. Wang, "Quantum electrodynamics near a photonic band gap: photon bound states and dressed atoms," Phys. Rev. Lett. **58,** 2418–2421 (1990).
5. S. L. McCall, P. M. Platzman, R. Dalichaouch, D. Smith, and S. Schultz, "Microwave propagation in two-dimensional dielectric lattices," Phys. Rev. Lett. **67,** 2017–2020 (1991).
6. A. Chelnokov, S. Rowson, J. M. Lourtioz, L. Duvillaret, and J. L. Coutaz, "Terahertz characterisation of mechanically machined 3D photonic crystal," Electron. Lett. **33,** 1981–1983 (1997).
7. J. E. G. J. Wijnhoven and W. L. Vos, "Preparation of photonic crystals made of air spheres in titania," Science **281,** 802–804 (1998).
8. H.-Y. Lee and T. Yao, "Design and evaluation of omnidirectional one-dimensional photonic crystals," J. Appl. Phys. **93,** 819–830 (2003).
9. K. M. Chen, A. W. Sparks, H. C. Luan, D. R. Lim, K. Wada, and L. C. Kimerling, "SiO_2/TiO_2 omnidirectional reflector and microcavity resonator via the sol-gel method," Appl. Phys. Lett. **75,** 3805–3807 (1999).
10. B. Temelkuran and E. Özbay, "Experimental demonstration of photonic crystal-based waveguides," Appl. Phys. Lett. **74,** 486–488 (1999).
11. A. Chelnokov, S. Rowson, J. M. Lourtioz, L. Duvillaret, and J. L. Coutaz, "Light controllable defect modes in three-dimensional photonic crystal," Electron. Lett. **34,** 1965–1967 (1998).
12. S. Y. Lin and G. Arjavalingam, "Photonic bound states in two-dimensional photonic crystals probed by coherent-microwave transient spectroscopy," J. Opt. Soc. Am. B **11,** 2124–2127 (1994).
13. W. M. Robertson, G. Arjavalingam, R. D. Meade, K. D. Brommer, A. M. Rappe, and J. D. Joannopoulos, "Measurement of photonic band structure in a two-dimensional periodic dielectric array," Phys. Rev. Lett. **68,** 2023–2026 (1992).
14. W. M. Robertson, G. Arjavalingam, R. D. Meade, K. D. Brommer, A. M. Rappe, and J. D. Joannopoulos, "Measurement of the photon dispersion relation in two-dimensional ordered dielectric arrays," J. Opt. Soc. Am. B **10,** 322–327 (1993).
15. T. Aoki, M. W. Takeda, J. W. Haus, Z. Yuan, M. Tani, K. Sakai, N. Kawai, and K. Inoue, "Terahertz time-domain study of a pseudo-simple-cubic photonic lattice," Phys. Rev. B **64,** 045106 (2001).
16. H. Kitahara, N. Tsumura, H. Kondo, M. W. Takeda, J. W. Haus, and Z. Yuan, "Terahertz wave dispersion in two-dimensional photonic crystals," Phys. Rev. B **64,** 045202 (2001).
17. P. L. Phillips, J. C. Knight, J. M. Pottage, G. Kakarantzas, and P. St. J. Russell, "Direct measurement of optical phase in the near field," Appl. Phys. Lett. **76,** 541–543 (2000).
18. N. Tsurumachi, S. Yamashita, N. Muroi, T. Fuji, T. Hattori, and H. Nakatsuka, "Enhancement of nonlinear optical effect in one-dimensional photonic crystal structures," Jpn. J. Appl. Phys. Part 1 **38,** 6302–6308 (1999).
19. E. Özbay and B. Temelkuran, "Reflection properties and defect formation in photonic crystals," Appl. Phys. Lett. **69,** 743–745 (1996).
20. B. Temelkuran, E. Özbay, M. Sigalas, G. Tuttle, C. M. Soukoulis, and K. M. Ho, "Reflection properties of metallic photonic crystals," Appl. Phys. A **66,** 363–365 (1998).
21. H. Němec, L. Duvillaret, F. Quemeneur, and P. Kužel, "Defect modes due to twinning in one-dimensional photonic crystals," J. Opt. Soc. Am. B (to be published).
22. G. Grüner, ed., *Millimeter and Submillimeter-Wave Spectroscopy of Solids* (Springer–Verlag, Berlin, 1998).
23. T.-I. Jeon and D. Grischkowsky, "Characterization of optically dense, doped semiconductors by reflection THz time domain spectroscopy," Appl. Phys. Lett. **72,** 3032–3034 (1998).
24. A. Pashkin, M. Kempa, H. Němec, F. Kadlec, and P. Kužel, "Phase-sensitive time-domain terahertz reflection spectroscopy," Rev. Sci. Instrum. **74,** 4711–4717 (2003).
25. A. Figotin and V. Gorentsveig, "Localized electromagnetic waves in a layered periodic dielectric medium with a defect," Phys. Rev. B **58,** 180–188 (1998).
26. S. F. Mingaleev and K. Busch, "Scattering matrix approach to large-scale photonic crystal circuits," Opt. Lett. **28,** 619–621 (2003).
27. M. Born and E. Wolf, *Principles of Optics*, 7th ed. (Cambridge U. Press, Cambridge, 1999), Chap. 1.6, pp. 54–74.
28. E. Yablonovitch, T. J. Gmitter, R. D. Meade, A. M. Rappe, K. D. Brommer, and J. D. Joannopoulos, "Donor and acceptor modes in photonic band structures," Phys. Rev. Lett. **67,** 3380–3383 (1991).
29. A. A. Asatryan, P. A. Robinson, L. C. Botten, R. C. McPhedran, N. A. Nicorovici, and C. M. de Sterke, "Effects of disorder on wave propagation in two-dimensional photonic crystals," Phys. Rev. E **60,** 6118–6127 (1999).
30. T. Hattori, N. Tsurumachi, S. Kawato, and H. Nakatsuka, "Photonic dispersion relation in a one-dimensional quasicrystal," Phys. Rev. B **50,** 4220–4223 (1994).
31. P. Kužel and J. Petzelt, "Time-resolved terahertz transmission spectroscopy of dielectrics," Ferroelectrics **239,** 949–956 (2000).
32. L. Duvillaret, F. Garet, and J.-L. Coutaz, "Influence of noise on the characterization of materials by terahertz time-domain spectroscopy," J. Opt. Soc. Am. B **17,** 452–461 (2000).
33. M. H. Lee and O. I. Sindoni, "Kramers–Kronig relations with logarithmic kernel and application to the phase spectrum in the Drude model," Phys. Rev. E **56,** 3891–3896 (1997).